Efficient Boundary Integral Equation Method for Photonic Crystal Fibers

Wangtao Lu and Ya Yan Lu

***Abstract*—Photonic crystal fibers (PCFs) with many air holes and complicated geometries can be difficult to analyze using conventional waveguide mode solvers such as the finite element method. Boundary integral equation (BIE) methods are suitable for PCFs, since they formulate eigenvalue problems only on the interfaces and are capable of computing leaky modes accurately. To improve the efficiency, it is desirable to have high order BIE methods that calculate the minimum number of functions on the interfaces. Existing BIE methods calculate two or four functions on the interfaces, but high order implementations are only available for those with four functions. In this paper, a new high order BIE method is developed and it calculates two functions on the interfaces. Numerical results indicate that the new BIE method achieves exponential convergence and extremely high accuracy.**

I. Introduction

PHOTONIC crystal fibers (PCFs) [1] have been extensively investigated because of their unique optical properties. The propagation of light in a PCF is strongly controlled by the geometry of its cross section. To design PCFs for various applications, fast and accurate numerical simulations are needed. Although many numerical methods are available, accurate analysis of light propagation in PCFs with large number of holes or complicated geometries remains quite difficult.

As a special class of optical waveguides, PCFs can be analyzed by existing numerical methods for optical waveguides, such as the finite difference method [2]–[4], the finite element method (FEM) [5]–[10], the multidomain pseudospectral method [11]–[13], the boundary integral equation (BIE) method [14]–[21], etc. Numerical methods that discretize the cross sections of PCFs, such as the FEM, give rise to linear matrix eigenvalue problems. However, if the PCF has many holes and complicated geometries, the size of the matrices can be very large and the matrix eigenvalue problem is expensive to solve. Furthermore, PCFs often have leaky modes. The electromagnetic field of a leaky mode exhibits outgoing wave behavior away from the waveguide core. Standard numerical methods must truncate the cross sections with proper absorbing boundary conditions, such as the perfectly matched layer (PML). To accurately calculate the small imaginary part of the complex propagation constant β of a leaky mode, the parameters of the PML must be carefully tuned.

The BIE method and the multipole method [22]–[28] give rise to a nonlinear eigenvalue problem

$$F(\beta)\phi = 0, \tag{1}$$

where the matrix F depends on β nonlinearly, but the size of F is much smaller. The multipole method is most suitable for PCFs with well-separated and circular air holes, it is less effective if the holes are close to each other, or the holes are non-circular, and if there are too many holes. The BIE method has been applied to study some complicated PCFs [16], [19], [20]. It can easily find leaky modes, since the outgoing radiation condition is automatically satisfied. Compared with the matrices in numerical methods that discretize the cross sections, the size of the matrix F is much smaller, since ϕ represents a few functions defined on the material interfaces only, but it still can be very significant if the PCF has many air holes and complicated geometries. To reduce the size of matrix F, a high order BIE method that uses the smallest number of functions on the material interfaces is desired. Existing high order BIE methods [15], [19], [20] solve four functions on the interfaces. BIE formulations that solve two functions on the interfaces exist [14], [16], but they do not have a high order of accuracy.

In this paper, we develop an efficient high order BIE method that solves two functions (the transverse components of the magnetic field) on the material interfaces. The key step is to use the kernel-splitting technique for discretizing the hypersingular boundary integral operators [29]. Numerical results indicate that our method achieves exponential convergence and extremely high accuracy.

II. Problem Formulation

We consider a PCF shown schematically in Fig. 1. It has a z-independent and piecewise constant refractive index function $n(x, y)$, where $\{x, y, z\}$ is a Cartesian coordinate system, the z-axis is the axis of the fiber, and the xy-plane is its cross section. The PCF consists of a finite number l_* of homogeneous inclusions embedded in a homogeneous background material. The cross sections of these homogeneous inclusions are the domains Ω_l, $1 \le l \le l_*$, in the xy-plane, and their exterior is the infinite domain Ω_0. The boundaries of these domains, denoted as $\partial\Omega_l$, are assumed to be smooth. The refractive indices of the inclusions and the background material are n_c and n_g, respectively. For simplicity, we assume

This work was partially supported by a grant from City University of Hong Kong (project no. 7008107).

W. Lu is with the Joint Advanced Research Center of University of Science and Technology of China and City University of Hong Kong, Suzhou, Jiangsu 215006, China, also with the School of Mathematical Sciences, University of Science and Technology of China, Hefei 230026, China, and also with the Department of Mathematics, City University of Hong Kong, Kowloon, Hong Kong.

Y. Y. Lu is with the Department of Mathematics, City University of Hong Kong, Kowloon, Hong Kong (e-mail: mayylu@cityu.edu.hk).

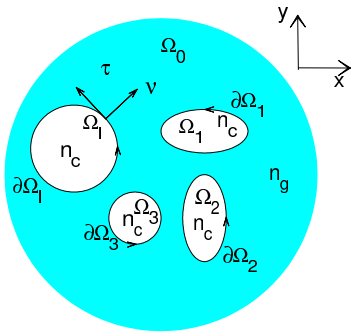

Fig. 1. Schematic of a PCF cross section.

all inclusions have the same refractive index, but our method is applicable to the more general case where different inclusions may have different indices.

Assuming the time dependence is $\exp(-i\omega t)$ where ω is the angular frequency, a propagating mode of a PCF is a special solution of the Maxwell's equations with the z dependence $\exp(i\beta z)$, where β is the propagation constant. If the mode is leaky, then β is complex, its electromagnetic field exhibits outgoing wave behavior as $|\boldsymbol{r}| = \sqrt{x^2+y^2} \to \infty$, and the imaginary part of β measures the attenuation of the mode along the fiber.

In each homogeneous domain Ω_l, $0 \le l \le l_*$, every component of the electromagnetic field of the mode satisfies the following Helmholtz equation

$$\partial_x^2 u + \partial_y^2 u + \gamma^2 u = 0, \tag{2}$$

where $\gamma^2 = k_0^2 n^2 - \beta^2$ and k_0 is the free space wavenumber. We formulate a nonlinear eigenvalue problem (1) where ϕ consists of H_x and H_y (transverse components of the magnetic field) on the interfaces, i.e. the boundaries of Ω_l for $1 \le l \le l_*$, or $\cup_{l=1}^{l_*} \partial\Omega_l$. To establish Eq. (1), we need to impose the conditions that E_z and H_z are continuous across the interfaces. Using the zero divergence property of the magnetic field, the condition on H_z leads to the continuity of $\partial_\nu H_\nu$ (normal derivative of the normal component of the magnetic field), where $\nu = (\nu_x, \nu_y)$ is a unit normal vector of $\partial\Omega_l$ directed into the exterior homogeneous domain. The Maxwell's equations give us $ik_0 n^2 E_z = \partial_y H_x - \partial_x H_y$. The partial derivatives with respect to x and y can be written as linear combinations of the normal and tangential derivatives. Therefore

$$\begin{bmatrix} ik_0 E_z \\ \partial_\nu H_\nu \end{bmatrix} = \mathcal{M} \begin{bmatrix} H_x \\ H_y \end{bmatrix} \tag{3}$$

where

$$\mathcal{M} = \begin{bmatrix} \frac{1}{n^2}(\nu_y \partial_\nu + \nu_x \partial_\tau) & \frac{1}{n^2}(\nu_y \partial_\tau - \nu_x \partial_\nu) \\ \nu_x \partial_\nu & \nu_y \partial_\nu \end{bmatrix}. \tag{4}$$

In the above, $\tau = (-\nu_y, \nu_x)$ is the unit tangential vector along $\partial\Omega_l$ and ∂_τ is the tangential derivative operator.

Clearly, in order to satisfy the continuity conditions on $\partial\Omega_l$, we need to match the inside and outside limits of the right hand side of (3) on $\partial\Omega_l$. This implies that we need to express $\partial_\nu H_x^{\pm}$, $\partial_\nu H_y^{\pm}$, $\partial_\tau H_x$ and $\partial_\tau H_y$ in terms of H_x and H_y on the interfaces. The tangential derivative is a local operator defined on $\partial\Omega_l$ and it can be approximated by a differentiation matrix. The normal derivatives of H_x and H_y are not continuous across $\partial\Omega_l$. For the inside limit of the normal derivative, we need to consider the Helmholtz equation (2) in Ω_l, where u is either H_x or H_y, and find an operator (the Dirichlet-to-Neumann (DtN) map) Λ_l, such that $\Lambda_l u = \partial_\nu u^-$ on $\partial\Omega_l$. For the outside limit of the normal derivative, we need to find the DtN map Λ_0 such that $\Lambda_0 u = \partial_\nu u^+$ on $\partial\Omega_0 = \cup_{l=1}^{l_*} \partial\Omega_l$ where u satisfies Eq. (2) in Ω_0. With the differentiation matrices for ∂_τ and the DtN maps, we can establish the nonlinear eigenvalue problem (1). In the next two sections, we present a high order method for computing the DtN maps by a BIE with a hypersingular integral operator.

III. Interior DtN Map

In a bounded domain Ω_l, $1 \le l \le l_*$, with a smooth boundary $\partial\Omega_l$, a function u satisfying the Helmholtz equation (2) has the following Green's representation formula:

$$u(\boldsymbol{r}) = \int_{\partial\Omega_l} \left[G(\boldsymbol{r}, \tilde{\boldsymbol{r}}) \partial_\nu u(\tilde{\boldsymbol{r}}) - \frac{\partial G(\boldsymbol{r}, \tilde{\boldsymbol{r}})}{\partial \nu(\tilde{\boldsymbol{r}})} u(\tilde{\boldsymbol{r}}) \right] ds(\tilde{\boldsymbol{r}}) \tag{5}$$

for $\boldsymbol{r} \in \Omega_l$, where ν is an outward normal vector of $\partial\Omega_l$, G is the Green's function of Eq. (2), i.e.,

$$G(\boldsymbol{r}, \tilde{\boldsymbol{r}}) = \frac{i}{4} H_0^{(1)}(\gamma |\boldsymbol{r} - \tilde{\boldsymbol{r}}|), \quad \boldsymbol{r} \ne \tilde{\boldsymbol{r}}, \tag{6}$$

$H_0^{(1)}$ is the zeroth order Hankel function of the first kind, $\boldsymbol{r} = (x, y)$ and $\tilde{\boldsymbol{r}} = (\tilde{x}, \tilde{y})$. Taking a limit for $\boldsymbol{r}$ to the boundary $\partial\Omega_l$, we obtain a BIE

$$(1 + \mathcal{K}) u = \mathcal{S} \partial_\nu u \quad \text{on} \quad \partial\Omega_l, \tag{7}$$

where $\mathcal{S}$ and $\mathcal{K}$ are boundary integral operators defined as

$$(\mathcal{S}\psi)(\boldsymbol{r}) = 2 \int_{\partial\Omega_l} G(\boldsymbol{r}, \tilde{\boldsymbol{r}}) \psi(\tilde{\boldsymbol{r}}) ds(\tilde{\boldsymbol{r}}), \quad \boldsymbol{r} \in \partial\Omega_l,$$
$$(\mathcal{K}\psi)(\boldsymbol{r}) = 2 \int_{\partial\Omega_l} \frac{\partial G(\boldsymbol{r}, \tilde{\boldsymbol{r}})}{\partial \nu(\tilde{\boldsymbol{r}})} \psi(\tilde{\boldsymbol{r}}) ds(\tilde{\boldsymbol{r}}), \quad \boldsymbol{r} \in \partial\Omega_l.$$

Taking a normal derivative of Eq. (5) and then a limit to the boundary, we get another BIE

$$(1 - \mathcal{K}') \partial_\nu u = -\mathcal{T} u \quad \text{on} \quad \partial\Omega_l, \tag{8}$$

where $\mathcal{K}'$ and $\mathcal{T}$ satisfy

$$(\mathcal{K}'\psi)(\boldsymbol{r}) = 2 \int_{\partial\Omega_l} \frac{\partial G(\boldsymbol{r}, \tilde{\boldsymbol{r}})}{\partial \nu(\boldsymbol{r})} \psi(\tilde{\boldsymbol{r}}) ds(\tilde{\boldsymbol{r}}), \quad \boldsymbol{r} \in \partial\Omega_l,$$
$$(\mathcal{T}\psi)(\boldsymbol{r}) = 2 \int_{\partial\Omega_l} \frac{\partial^2 G(\boldsymbol{r}, \tilde{\boldsymbol{r}})}{\partial \nu(\boldsymbol{r}) \partial \nu(\tilde{\boldsymbol{r}})} \psi(\tilde{\boldsymbol{r}}) ds(\tilde{\boldsymbol{r}}), \quad \boldsymbol{r} \in \partial\Omega_l.$$

The boundary integral operators $\mathcal{S}$, $\mathcal{K}$ and $\mathcal{K}'$ are compact operators with eigenvalues accumulating at zero [30]. When discretized, these operators are approximated by near singular matrices. Therefore, it is numerically unstable to calculate the DtN map by $\Lambda_l = \mathcal{S}^{-1}(1 + \mathcal{K})$. Except when $\mathcal{K}'$ has an eigenvalue exactly equal to 1, the operator $1 - \mathcal{K}'$ has a bounded inverse and we can calculate the DtN map by $\Lambda_l = -(1 - \mathcal{K}')^{-1} \mathcal{T}$. However, $\mathcal{T}$ is a hypersingular operator [30] and it is more difficult to approximate. Fortunately, when $\partial\Omega_l$ is smooth, an accurate discretization of $\mathcal{T}$ was developed

by Kress [29] based on a Nyström method and a kernel-splitting technique. In the following, we apply the method of Kress to discretize Eq. (8) and find the DtN map.

Assuming $\partial\Omega_l$ has a parametric representation

$$\boldsymbol{r}(t) = [x(t), y(t)], \quad 0 \le t \le 2\pi, \tag{9}$$

where t increases in the counterclockwise direction of $\partial\Omega_l$, $x(t)$ and $y(t)$ are analytic and 2π-periodic functions of t, and $|\boldsymbol{r}'(t)| > 0$ for all t, then the operators $\mathcal{K}'$ and $\mathcal{T}$ can be written as

$$(\mathcal{K}'\partial_\nu u)(\boldsymbol{r}(t)) = \int_0^{2\pi} \frac{|\boldsymbol{r}'(\tilde{t})|}{|\boldsymbol{r}'(t)|} P(t,\tilde{t})\partial_\nu u(\boldsymbol{r}(\tilde{t}))d\tilde{t}, \tag{10}$$

$$(\mathcal{T}u)(\boldsymbol{r}(t)) = \frac{1}{|\boldsymbol{r}'(t)|}\int_0^{2\pi}\left\{\frac{1}{2\pi}\cot\frac{\tilde{t}-t}{2}u'(\boldsymbol{r}(\tilde{t})) - Q(t,\tilde{t})u(\boldsymbol{r}(\tilde{t}))\right\}d\tilde{t} \tag{11}$$

where P and Q are given in the appendix, $u'(\boldsymbol{r}(t))$ is the t-derivative of $u(\boldsymbol{r}(t))$. Thus, Eq. (8) can be written as

$$|\boldsymbol{r}'(t)|\partial_\nu u(\boldsymbol{r}(t)) - \int_0^{2\pi} P(t,\tilde{t})|\boldsymbol{r}'(\tilde{t})|\partial_\nu u(\boldsymbol{r}(\tilde{t}))d\tilde{t} = \int_0^{2\pi}\left[Q(t,\tilde{t})u(\boldsymbol{r}(\tilde{t})) - \frac{1}{2\pi}\cot\frac{\tilde{t}-t}{2}u'(\boldsymbol{r}(\tilde{t}))\right]d\tilde{t}. \tag{12}$$

To discretize the above equation, we first split out the logarithmic singularities in the kernels as

$$P(t,\tilde{t}) = P_1(t,\tilde{t})L(t,\tilde{t}) + P_2(t,\tilde{t}),$$
$$Q(t,\tilde{t}) = Q_1(t,\tilde{t})L(t,\tilde{t}) + Q_2(t,\tilde{t}),$$

where

$$L(t,\tilde{t}) = \log\left(4\sin^2\frac{t-\tilde{t}}{2}\right), \tag{13}$$

P_1, P_2, Q_1 and Q_2 are smooth functions given in the appendix, then use quadrature formulas based on a uniform discretization in t. Let ψ be an analytic and 2π-periodic function of t, and for a positive even integer N_l and $t_j = 2\pi j/N_l$ for $0 \le j < N_l$, we have the following three quadrature formulas [29]:

$$\int_0^{2\pi}\psi(\tilde{t})d\tilde{t} \approx \frac{2\pi}{N_l}\sum_{j=0}^{N_l-1}\psi(t_j),$$

$$\int_0^{2\pi}\psi(\tilde{t})L(t,\tilde{t})d\tilde{t} \approx \sum_{j=0}^{N_l-1}R_j(t)\psi(t_j),$$

$$\frac{1}{2\pi}\int_0^{2\pi}\cot\frac{\tilde{t}-t}{2}\psi'(\tilde{t})d\tilde{t} \approx \sum_{j=0}^{N_l-1}T_j(t)\psi(t_j),$$

where

$$R_j(t) = -\frac{4\pi}{N_l^2}\left[\sum_{m=1}^{N_l/2-1}\frac{2}{m}\cos m(t-t_j) + \cos\frac{N_l(t-t_j)}{2}\right],$$

$$T_j(t) = -\frac{1}{N_l}\left[\sum_{m=1}^{N_l/2-1}2m\cos m(t-t_j) + \cos\frac{N_l(t-t_j)}{2}\right].$$

The first formula is simply the trapezoidal rule. The other two formulas can be derived from a trigonometric interpolation of $\psi(t)$:

$$\psi(t) \approx \sum_{j=0}^{N_l-1}\left[\frac{1}{N_l}\sum_{k=-N_l/2}^{N_l/2-1}e^{ik(t-t_j)}\right]\psi(t_j). \tag{14}$$

Approximating the integrals in Eq. (12) by the quadrature formulas and collocating t at t_j for $0 \le j < N_l$, we obtain a linear system that can be solved to give a matrix Λ_l such that

$$\partial_\nu\boldsymbol{u} = \Lambda_l\boldsymbol{u}, \tag{15}$$

where $\partial_\nu\boldsymbol{u}$ and $\boldsymbol{u}$ denote the column vectors of $\partial_\nu u(\boldsymbol{r}(t_j))$ and $u(\boldsymbol{r}(t_j))$ for $0 \le j < N_l$.

IV. Exterior DtN map

For the exterior homogeneous domain Ω_0, u and $\partial_\nu u$ satisfy

$$(1+\mathcal{K}')\partial_\nu u = \mathcal{T}u \quad \text{on} \quad \partial\Omega_0, \tag{16}$$

where the integral operators $\mathcal{K}'$ and $\mathcal{T}$ are now defined on l_* closed curves as

$$(\mathcal{K}'\psi)(\boldsymbol{r}) = 2\sum_{l=1}^{l_*}\int_{\partial\Omega_l}\frac{\partial G(\boldsymbol{r},\tilde{\boldsymbol{r}})}{\partial\nu(\boldsymbol{r})}\psi(\tilde{\boldsymbol{r}})ds(\tilde{\boldsymbol{r}}), \tag{17}$$

$$(\mathcal{T}\psi)(\boldsymbol{r}) = 2\sum_{l=1}^{l_*}\int_{\partial\Omega_l}\frac{\partial^2 G(\boldsymbol{r},\tilde{\boldsymbol{r}})}{\partial\nu(\boldsymbol{r})\partial\nu(\tilde{\boldsymbol{r}})}\psi(\tilde{\boldsymbol{r}})ds(\tilde{\boldsymbol{r}}), \tag{18}$$

for $\boldsymbol{r} \in \partial\Omega_0$. We take the integration along $\partial\Omega_1$ for any point $\boldsymbol{r}_0 \in \partial\Omega_0$ to illustrate the basic ideas for discretizing $\mathcal{K}'$ and $\mathcal{T}$. Assuming $\partial\Omega_1 = \{\boldsymbol{r}(t) \mid 0 \le t \le 2\pi\}$ is discretized by N_1 points corresponding to $\{t_j = 2\pi j/N_1\}_{j=0}^{N_1-1}$, we need to evaluate the integral

$$g(\boldsymbol{r}_0) = \int_0^{2\pi}\Phi(\boldsymbol{r}_0,t)\psi(t)|\boldsymbol{r}'(t)|dt, \tag{19}$$

where $\psi(t)$ denotes $\psi(\boldsymbol{r}(t))$, and

$$\Phi(\boldsymbol{r}_0,t) = \frac{\partial G(\boldsymbol{r}_0,\boldsymbol{r}(t))}{\partial\nu(\boldsymbol{r}_0)} \quad \text{or}$$
$$\Phi(\boldsymbol{r}_0,t) = \frac{\partial^2 G(\boldsymbol{r}_0,\boldsymbol{r}(t))}{\partial\nu(\boldsymbol{r}_0)\partial\nu(\boldsymbol{r})}.$$

We distinguish three cases. The first case is when $\boldsymbol{r}_0 \in \partial\Omega_1$, the integration kernels are singular at $\boldsymbol{r}(t) = \boldsymbol{r}_0$. We can use the discretization process described in the previous section. If $\boldsymbol{r}_0 \notin \partial\Omega_1$, then the distance between $\boldsymbol{r}_0$ and $\partial\Omega_1$, denoted by $\text{dist}(\boldsymbol{r}_0,\partial\Omega_1)$, is positive. The second case is when $\text{dist}(\boldsymbol{r}_0,\partial\Omega_1)$ is larger than some constant $c > 0$. As an empirical rule, we take $c = \lambda$ in our numerical examples, where λ is the free space wavelength. In that case, a simple trapezoidal rule can be applied to discretize (19), that is,

$$g(\boldsymbol{r}_0) \approx \frac{2\pi}{N_1}\sum_{j=0}^{N_1-1}\Phi(\boldsymbol{r}_0,t_j)\psi(t_j)|\boldsymbol{r}'(t_j)|. \tag{20}$$

The last case is when $\text{dist}(\boldsymbol{r}_0,\partial\Omega_1) \le c$. The trapezoidal rule (20) is no longer accurate. We follow the method described in

[20]. Substituting the trigonometric interpolation of $\psi(t)$, i.e., Eq. (14), into (19), we get

$$g(\boldsymbol{r}_0) \approx \frac{1}{N_1} \sum_{j=0}^{N_1-1} \sum_{k=-N_1/2}^{N_1/2-1} e^{-ikt_j} g_k(\boldsymbol{r}_0)\psi(t_j),$$

where

$$g_k(\boldsymbol{r}_0) = \int_0^{2\pi} \Phi(\boldsymbol{r}_0, t)e^{ikt}|\boldsymbol{r}'(t)|dt, \tag{21}$$

for $-N_1/2 \le k < N_1/2$. We still approximate (21) by the trapezoidal rule, but use a larger number of points for t and the Fast Fourier Transform (FFT) to speed up the evaluation.

Therefore, using the above procedure, we can discretize $\mathcal{K}'$ and $\mathcal{T}$, and obtain a matrix Λ_0 such that

$$\partial_\nu \boldsymbol{u} = \Lambda_0 \boldsymbol{u}, \tag{22}$$

where $\boldsymbol{u}$ and $\partial_\nu \boldsymbol{u}$ denote column vectors of length $N_{all} = \sum_{l=1}^{l_*} N_l$ for u and $\partial_\nu u$ on $\partial\Omega_0$.

V. Equation for β

Using the DtN maps Λ_l ($1 \le l \le l_*$) and Λ_0, we are able to express $\partial_\nu H_x^-$, $\partial_\nu H_y^-$ and $\partial_\nu H_x^+$, $\partial_\nu H_y^+$ in terms of H_x and H_y on the interfaces. The interface conditions given in (3) also require the evaluation of tangential derivatives along $\partial\Omega_l$. For a smooth function $\psi(\boldsymbol{r})$ given on the boundary $\partial\Omega_l$, we use the trigonometric interpolation of $\psi(t) = \psi(\boldsymbol{r}(t))$ as given in (14) to approximate the derivative with respect to t. That is

$$\psi'(t) \approx \sum_{j=0}^{N_l-1} \left[\frac{i}{N_l} \sum_{k=-N_l/2}^{N_l/2-1} k e^{ik(t-t_j)} \right] \psi(t_j). \tag{23}$$

Evaluating the above at $\{t_0, t_1, ..., t_{N_l-1}\}$ and using the relation $\psi'(t) = |\boldsymbol{r}'(t)|\partial_\tau \phi(\boldsymbol{r}(t))$, we can find the differentiation matrix $\mathcal{D}_l$, such that

$$\partial_\tau \boldsymbol{\psi} = \mathcal{D}_l \boldsymbol{\psi}, \tag{24}$$

where $\partial_\tau \boldsymbol{\psi}$ and $\boldsymbol{\psi}$ are column vectors of length N_l for $\partial_\tau \psi(\boldsymbol{r}(t))$ and $\psi(\boldsymbol{r}(t))$ at the N_l points. Using the DtN maps and the differentiation matrices, we can match the right hand side of (3) from inside and outside Ω_l, $1 \le l \le l_*$, and establish the nonlinear eigenvalue problem (1), where $F(\beta)$ is a $(2N_{all}) \times (2N_{all})$ matrix and N_{all} is the total number of discretization points on all interfaces.

A mode of the PCF corresponds to a value of β for which the matrix $F(\beta)$ is singular. A common measure of the singularity is the determinant of $F(\beta)$, but it is not always reliable. Other measures include the smallest eigenvalue (in magnitude) and the smallest singular value, but they are relatively expensive to calculate. As in [19], we solve β from the equation

$$f(\beta) = \frac{1}{\boldsymbol{a}^T F^{-1}(\beta)\boldsymbol{b}} = 0 \tag{25}$$

using Müller's method, where $\boldsymbol{a}$ and $\boldsymbol{b}$ are two fixed random column vectors. In each iteration, we need to find $\boldsymbol{w} = F^{-1}(\beta)\boldsymbol{b}$ by solving the linear system $F(\beta)\boldsymbol{w} = \boldsymbol{b}$.

VI. Numerical Examples

In this section, we illustrate our method by a few examples. For the two simple examples shown in Fig. 2, we perform

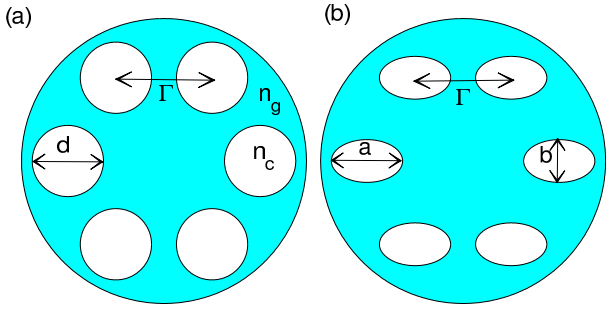

Fig. 2. Two simple PCFs: (a) six circular holes, parameters: diameter $d = 5\mu m$, pitch $\Gamma = 6.75\,\mu$m; (b) six elliptic holes, parameter: major axis $a = 5\,\mu$m, minor axis $b = 3\,\mu$m, pitch $\Gamma = 6.75\,\mu$m. The medium surrounding the holes is infinite.

numerical convergence tests and accuracy comparisons. The first example is a PCF with six circular air holes as shown in Fig. 2(a), and it has been analyzed by a number of authors [13], [19], [20]. The PCF consists of a single ring of six circular holes with diameters $d = 5\,\mu$m symmetrically arranged around the core with a pitch $\Gamma = 6.75\,\mu$m. The refractive indices of the glass matrix and the air hole are $n_g = 1.45$ and $n_c = 1$, respectively. The free space wavelength for this example is $\lambda = 1.45\,\mu$m. Using 80 points on the boundary of each hole, we obtain an accurate solution $\beta/k_0 = 1.4453952321493 + 3.194529\text{E}{-8}i$ for the fundamental mode of this PCF. Our result agrees well with the result of Chiang *et al.* [13] ($\beta/k_0 = \underline{1.44539525}694857 + \underline{3.194}695\text{E}{-8}i$), the result of White *et al.* [26] ($\beta/k_0 = \underline{1.445395}345 + \underline{3.15}\text{E}{-8}i$) and the result of Cheng *et al.* [19] ($\beta/k_0 = \underline{1.445395232} + \underline{3.1945}\text{E}{-8}i$). Using our solution above as a reference, we calculate the absolute errors in the real and imaginary parts of β/k_0 for the numerical solutions computed with a smaller number of discretization points. The results are shown in Fig. 3. The errors decrease exponentially from 30 to 50 points on each boundary, and they turn over to round off errors when the number of points is more than 50.

The second example, as shown in Fig. 2(b), has six elliptic air holes with major axis $a = 5\,\mu$m and minor axis $b = 3\,\mu$m. The other parameters are identical to the first example. We calculate its fundamental mode using 80 discretization points on the boundary of each hole. Our result is $\beta/k_0 = 1.44642907238417 + 2.9898269\text{E}{-6}i$, and it agrees very well with the result of Pone *et al.* [20] ($\beta/k_0 = \underline{1.446429072} + \underline{2.9898}\text{E}{-6}i$) and the result of Campbell *et al.* [28] ($\beta/k_0 = \underline{1.446427}235 + \underline{2.96}01\text{E}{-6}i$). Using our solution above as a reference, we calculate absolute errors for other numerical solutions and plot the convergence curves in Fig. 4. Once again, an exponential convergence is observed.

The third example is a PCF with six cookie-shaped air holes as shown in Fig. 5. For $1 \le j \le 6$, the boundary of the jth hole is given by

$$\boldsymbol{r}(t) = [x_j - p(t)\cos(t), y_j - p(t)\sin(t)], \quad 0 \le t \le 2\pi, \tag{26}$$

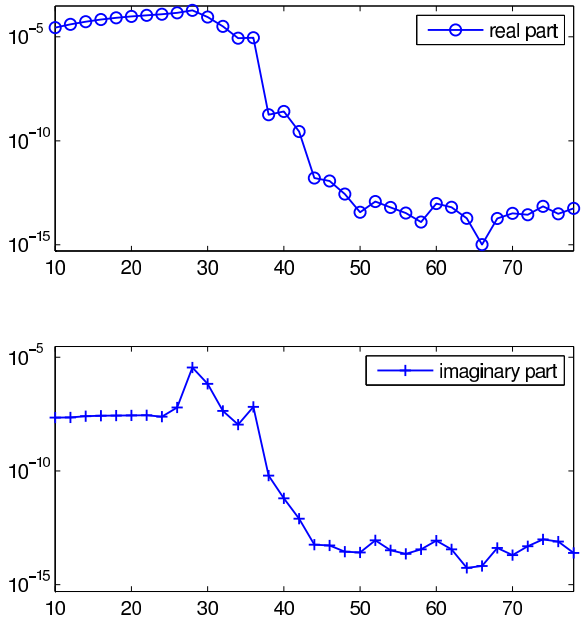

Fig. 3. Convergence curves for the fundamental mode of the PCF in Fig. 2(a).

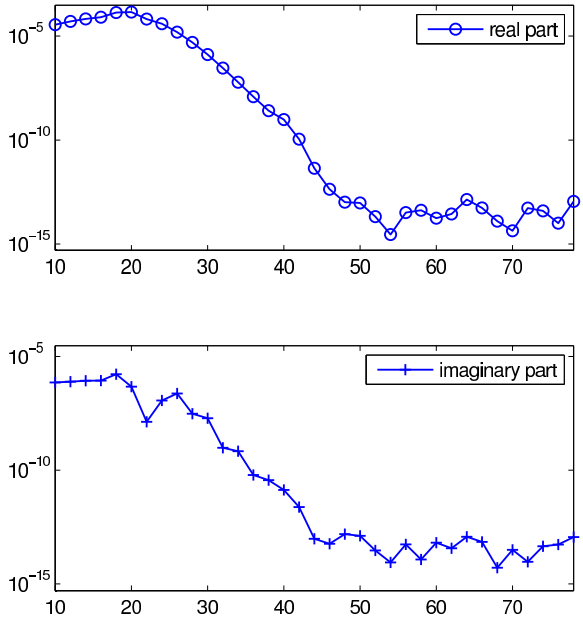

Fig. 4. Convergence curves for the fundamental mode of the PCF in Fig. 2(b).

where $\boldsymbol{r}_j^c = (x_j, y_j)$ is the center of the jth hole, and

$$p(t) = 2.5 + 0.15\sin(7t). \tag{27}$$

The other parameters, i.e., Γ, n_g, n_c and λ, are identical to the first two examples. This PCF was previously analyzed by Cheng *et al.* [19]. We calculate the two fundamental modes for this PCF. The numerical results are listed in Tabel I and Table II, where N denotes the number of discretization points on the boundary of each hole. The results reported in [19] are $\beta/k_0 = \underline{1.445343940} + \underline{2.5019}\text{E}{-8}i$ and $\beta/k_0 = \underline{1.445343873} + \underline{2.5056}\text{E}{-8}i$ for the first and second modes, respectively. The agreement is excellent.

The fourth and fifth examples are more complex PCFs

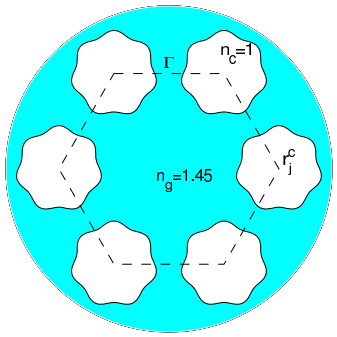

Fig. 5. A PCF with six cookie-shaped air holes where $\Gamma = 6.75\,\mu$m.

N	β/k_0
70	$1.4453434192003 + 2.59021\text{E}{-8}i$
80	$1.4453439283812 + 2.48475\text{E}{-8}i$
90	$1.4453439401195 + 2.49990\text{E}{-8}i$
100	$1.4453439397734 + 2.50177\text{E}{-8}i$
110	$1.4453439395692 + 2.50183\text{E}{-8}i$
120	$1.4453439395666 + 2.50182\text{E}{-8}i$

TABLE I
EXAMPLE 3: NUMERICAL SOLUTIONS OF β/k_0 FOR THE FIRST FUNDAMENTAL MODE.

shown in Fig. 6 and they have been previously analyzed by

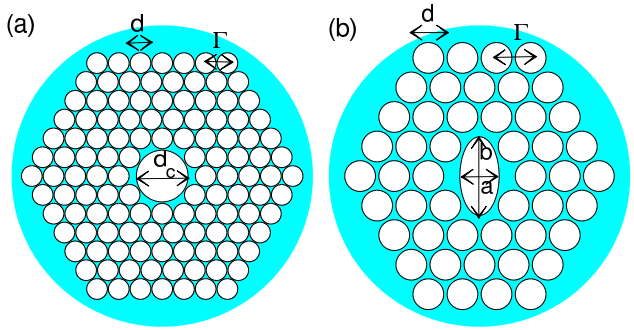

Fig. 6. Two complex PCFs: (a) hollow core PCF with five rings of circular holes, parameters: pitch $\Gamma = 2.74\,\mu$m, hole diameter $d = 0.95\Gamma$, core diameter $d_c = 2.5d$. (b) elliptic hollow core PCF with three layers of circular holes, parameters: pitch $\Gamma = 2\,\mu$m, hole diameter $d = 0.9\Gamma$, core principle axes $a = 2.3\,\mu$m and $b = 4.6\,\mu$m. The medium surrounding the holes is infinite.

Pone *et al.* [20]. The fourth example shown in Fig.6(a) is a PCF consisting of five rings of circular holes arranged on a hexagonal lattice and surrounding a hollow core formed by the two missing rings in the fiber center. The pitch is $\Gamma = 2.74\,\mu$m, the diameter of the small holes is $d = 0.95\Gamma$, and the diameter

N	β/k_0
70	$1.4453433575038 + 2.59745\text{E}{-8}i$
80	$1.4453438625539 + 2.48831\text{E}{-8}i$
90	$1.4453438734906 + 2.50366\text{E}{-8}i$
100	$1.4453438731792 + 2.50554\text{E}{-8}i$
110	$1.4453438729300 + 2.50558\text{E}{-8}i$
120	$1.4453438729292 + 2.50558\text{E}{-8}i$

TABLE II
EXAMPLE 3: NUMERICAL SOLUTIONS OF β/k_0 FOR THE SECOND FUNDAMENTAL MODE.

of the core is $d_c = 2.5d$. Overall, there are 120 small holes and one big hole (the hollow core). The refractive indices of the glass matrix and the air hole are $n_g = 1.45$ and $n_c = 1$, respectively. We calculate the fundamental mode of this PCF for free space wavelength $\lambda = 1.51\mu m$. The results are listed in Table III. The integers in the first and second columns represent the numbers of the discretization points for the big hole and the smaller holes, respectively. Our results agree well with the result of Pone *et al.* [20] ($\beta/k_0 = \underline{0.98451599}741954 + \underline{3.4}34721\text{E}{-8}i$). It appears that our solution in the first row of Table III is more accurate than that of Pone *et al.* [20]. In that case, the size of matrix F is $(34 \times 120 + 100) \times 2 = 8360$ and it is smaller than the matrix size 12544 used in [20].

N_1	N_2	β/k_0
100	34	$0.984516001097 + 3.41090\text{E}{-8}i$
120	40	$0.984516001952 + 3.41151\text{E}{-8}i$
120	42	$0.984516001485 + 3.41155\text{E}{-8}i$
120	46	$0.984516000680 + 3.41147\text{E}{-8}i$
120	50	$0.984516000835 + 3.41133\text{E}{-8}i$
120	60	$0.984516000835 + 3.41147\text{E}{-8}i$

TABLE III
EXAMPLE 4: SEVERAL VALUES OF β/k_0 FOR DIFFERENT NUMBER OF DISCRETIZATION POINTS.

Finally, we consider the PCF shown in Fig.6(b). It consists of three layers of circular holes arranged on a hexagonal lattice. The four missing holes at the center of the fiber are replaced by a central elliptic core. The hole pitch is $\Gamma = 2\,\mu$m, the hole diameter is $d = 0.9\Gamma$, the minor and major axes of the elliptic core are $a = 2.3\,\mu$m and $b = 4.6\,\mu$m, respectively. The refractive indices of the glass matrix and the air hole are $n_g = 1.45$ and $n_c = 1$. We calculate the two fundamental modes (the x and y polarizations, respectively) for free space wavelength $\lambda = 1.42\,\mu$m. The results are shown in Table IV and Table V. The first and second columns are the numbers of points used for the elliptic core and the circular holes, respectively. Compared with the two results given in [20] ($\beta/k_0 = \underline{0.93903355} + \underline{6.7418}\text{E}{-4}i$ and $\beta/k_0 = \underline{0.93816250} + \underline{2.2133}\text{E}{-3}i$ for the x and y polarizations, respectively), it is clear that our solutions are more accurate.

N_1	N_2	β/k_0
120	40	$0.9390335473927 + 6.741806549\text{E}{-4}i$
120	44	$0.9390335474024 + 6.741806722\text{E}{-4}i$
120	50	$0.9390335474106 + 6.741806729\text{E}{-4}i$
120	60	$0.9390335474115 + 6.741806730\text{E}{-4}i$

TABLE IV
EXAMPLE 5: SEVERAL VALUES OF β/k_0 FOR THE x POLARIZATION AND FOR DIFFERENT NUMBER OF DISCRETIZATION POINTS.

N_1	N_2	β/k_0
150	40	$0.9381625149831 + 2.213306320\text{E}{-3}i$
150	44	$0.9381625147761 + 2.213306371\text{E}{-3}i$
150	50	$0.9381625147583 + 2.213306378\text{E}{-3}i$
150	60	$0.9381625147578 + 2.213306378\text{E}{-3}i$

TABLE V
EXAMPLE 5: SEVERAL VALUES OF β/k_0 FOR THE y POLARIZATION AND FOR DIFFERENT NUMBER OF DISCRETIZATION POINTS.

VII. CONCLUSION

A new high order BIE mode solver is developed for PCFs with smooth interfaces. The method achieves exponential convergence, solves two functions on the interfaces and is more efficient than existing BIE methods [14]–[16], [19], [20]. Existing high order BIE methods [15], [19], [20] solve four functions on the interfaces. On the other hand, existing BIE methods that solve two functions on the interfaces have only low-order implementations. Our high order BIE method relies on the Nyström method and kernel-splitting technique developed by Kress [29] for discretizing hypersingular integral operators. Very accurate solutions are obtained for some rather complicated PCFs. Numerical results also indicate that the errors decrease exponentially with the number of points used.

APPENDIX

The kernel functions P and Q are given by

$$P(t,\tilde{t}) = \frac{i\gamma\rho(t,\tilde{t})}{2d(t,\tilde{t})} H_1^{(1)}(\gamma d(t,\tilde{t})), \quad (28)$$

$$Q(t,\tilde{t}) = N(t,\tilde{t}) - \gamma^2 M(t,\tilde{t})\boldsymbol{n}(t)\cdot\boldsymbol{n}(\tilde{t}), \quad (29)$$

where

$$\begin{aligned}
\boldsymbol{n}(t) &= |\boldsymbol{r}'(t)|\,\nu(\boldsymbol{r}(t)),\\
d(t,\tilde{t}) &= |\boldsymbol{r}(t) - \boldsymbol{r}(\tilde{t})|,\\
\rho(t,\tilde{t}) &= \boldsymbol{n}(t)\cdot[\boldsymbol{r}(\tilde{t}) - \boldsymbol{r}(t)],\\
M(t,\tilde{t}) &= \frac{i}{2} H_0^{(1)}(\gamma d(t,\tilde{t})),\\
N(t,\tilde{t}) &= \frac{1}{2\pi}\frac{\partial^2}{\partial t\partial\tilde{t}}\left\{ i\pi H_0^{(1)}(\gamma d(t,\tilde{t})) + L(t,\tilde{t})\right\}
\end{aligned}$$

and $L(t,\tilde{t})$ is given in (13). The logarithmic singularity is spitted as follows

$$P(t,\tilde{t}) = P_1(t,\tilde{t})L(t,\tilde{t}) + P_2(t,\tilde{t}), \quad (30)$$

$$M(t,\tilde{t}) = M_1(t,\tilde{t})L(t,\tilde{t}) + M_2(t,\tilde{t}), \quad (31)$$

$$N(t,\tilde{t}) = N_1(t,\tilde{t})L(t,\tilde{t}) + N_2(t,\tilde{t}), \quad (32)$$

where

$$\begin{aligned}
P_1(t,\tilde{t}) &= -\frac{\gamma\rho(t,\tilde{t})}{2\pi d(t,\tilde{t})} J_1(\gamma d(t,\tilde{t})),\\
M_1(t,\tilde{t}) &= -\frac{1}{2\pi} J_0(\gamma d(t,\tilde{t})),\\
N_1(t,\tilde{t}) &= -\frac{1}{2\pi}\frac{\partial^2}{\partial t\partial\tilde{t}} J_0(\gamma d(t,\tilde{t})).
\end{aligned}$$

The functions P_2, M_2 and N_2 can be evaluated using (30)-(32) except when $t = \tilde{t}$. In that case,

$$P_2(t,t) = \frac{1}{2\pi}\frac{\boldsymbol{n}(t)\cdot\boldsymbol{r}''(t)}{|\boldsymbol{r}'(t)|^2},$$
$$M_2(t,t) = \frac{i}{2} - \frac{C}{\pi} - \frac{1}{\pi}\ln\frac{\gamma|\boldsymbol{r}'(t)|}{2},$$
$$N_2(t,t) = \left(\pi i - 1 - 2C - 2\ln\frac{\gamma|\boldsymbol{r}'(t)|}{2}\right)\frac{\gamma^2|\boldsymbol{r}'(t)|^2}{4\pi} + \frac{1}{12\pi} + \frac{[\boldsymbol{r}'(t)\cdot\boldsymbol{r}''(t)]^2}{2\pi|\boldsymbol{r}'(t)|^4} - \frac{|\boldsymbol{r}''(t)|^2}{4\pi|\boldsymbol{r}'(t)|^2} - \frac{\boldsymbol{r}'(t)\cdot\boldsymbol{r}'''(t)}{6\pi|\boldsymbol{r}'(t)|^2},$$

where $C = 0.57721\cdots$ is the Euler's constant. The splitting for Q follows the splittings for M and N.

REFERENCES

[1] P. Russell, "Photonic crystal fibers," *Science*, vol. 299, no. 5605, pp. 358-362, Jan. 2003.

[2] G. R. Hadley, "High-accuracy finite-difference equations for dielectric waveguide analysis II: Dielectric corners," *J. Lightwave Technol.*, vol. 20, pp. 1219-1231, July 2002.

[3] N. Thomas, P. Sewell, T. M. Benson, "A new full-vectorial higher order finite-difference scheme for the modal analysis of rectangular dielectric waveguides," *J. Lightwave Technol.*, vol. 25, pp. 2563-2570, Sept. 2007.

[4] Y. P. Chiou, Y. C. Chiang, C. H. Lai, C. H. Du, and H. C. Chang, "Finite difference modeling of dielectric waveguides with corners and slanted facets," *J. Lightwave Technol.*, vol. 27, pp. 2077-2086, Dec. 2009.

[5] M. Koshiba and Y. Tsuji, "Curvilinear hybrid edge/nodal elements with triangular shape for guided-wave problems," *J. Lightwave Technol.*, vol. 18, pp. 737-743, May 2000.

[6] F. Brechet, J. Marcou, D. Pagnoux, and P. Roy, "Complete analysis of the characterisitics of propagation into photonic crystal fibers by the finite element method", *Opt. Fiber Technol.*, vol. 6, pp. 181-191, Apr. 2000.

[7] S. Selleri, L. Vincetti L, A. Cucinotta, and M. Zoboli, "Complex FEM modal solver of optical waveguides with PML boundary conditions," *Opt. Quant. Electron.*, vol. 33, pp. 359-371, 2001.

[8] S. S. A. Obayya, B. M. A. Rahman, K. T. V. Grattan, and H. A. El-Mikati, "Full vectorial finite-element-based imaginary distance beam propagation solution of complex modes in optical waveguides," *J. Lightwave Technol.*, vol. 20, pp. 1054-1060, June 2002.

[9] K. Saitoh, M. Koshiba, "Full-vectorial imaginary-distance beam propagation method based on a finite element scheme: application to photonic crystal fibers," *IEEE J. Quantum Electron.*, vol. 38, pp. 927-933, Jul. 2002.

[10] A. Cucinotta, S. Selleri, L. Vincent and M. Zoboli, "Holey fiber analysis through the finite element method," *IEEE Photon. Technol. Lett.*, vol. 14, pp. 1530-1532, Nov. 2002.

[11] C. C. Huang, C. C. Huang, and J. Y. Yang, "A full-vectorial pseudospectral modal analysis of dielectric optical waveguides with stepped refractive index profiles," *IEEE J. Sel. Top. Quantum Electron.*, vol. 11, pp. 457-465, 2005.

[12] P. J. Chiang, C. L. Wu, C. H. Teng, C. S. Yang, and H. C. Chang, "Full-vectorial optical waveguide mode solvers using multidomain pseudospectral frequency-domain (PSFD) formulations," IEEE J. Quantum Electron., vol. 44, pp. 56-66, 2008.

[13] P. Chiang and H. Chang, "A high-accuracy pseudospectral full-vectorial leaky optical waveguide mode solver with carefully implemented UPML absorbing boundary conditions," *Opt. Express*, vol. 19, pp. 1594-1608, Jan. 2011.

[14] C. C. Su, "A surface integral equations method for homogeneous optical fibers and coupled image lines of arbitrary cross sections," *IEEE Trans. Microwave Theory Tech.*, vol. 33, pp. 1114-1119, Nov. 1985.

[15] S. V. Boriskina, T. M. Benson, P. Sewell and A. I. Nosich, "Highly efficient full-vectorial integral equation solution for the bound, leaky and complex modes of dielectric waveguides," *IEEE J. Sel. Top. Quantum Electron.*, vol. 8, pp. 1225-1231, Nov. 2002.

[16] N. Guan, S. Habu, K. Takenaga, K. Himeno, and A. Wada, "Boundary Element Method for Analysis of Holey Optical Fibers," *J. Lightwave Technol.*, vol. 21, pp. 1787-1792, Aug. 2003.

[17] T. Lu and D. Yevick, "A vectorial boundary element method analysis of integrated optical waveguides," *J. Lightwave Technol.*, vol. 21, pp. 1793-1807, Aug. 2003.

[18] T. Lu and D. Yevick, "Comparative evaluation of a novel series approximation for electromagnetic fields at dielectric corners with boundary element method applications," *J. Lightwave Technol.*, vol. 22, pp. 1426-1432, May 2004.

[19] H. Cheng, W. Y. Crutchfield, M. Doery and L. Greengard, "Fast, accurate integral equation methods for the analysis of photonic crystal fibers I: Theory," *Opt. Express*, vol. 12, pp. 3791-3805, Aug. 2004.

[20] E. Pone, A. Hassani, S. Lacroix, A. Kabashin and M. Skorobogatiy, "Boundary integral method for the challenging problems in bandgap guiding, plasmonics and sensing," *Opt. Express*, vol. 15, pp. 10231-10246, Aug. 2007.

[21] W. Lu and Y. Y. Lu, "Waveguide mode solver based on Neumann-to-Dirichlet operators and boundary integral equations," *J. Comput. Phys.*, vol. 231, pp. 1360-1371, 2012.

[22] W. Wijngaard, "Guided normal modes of two parallel circular dielectric rods," *J. Opt. Soc. Am.*, vol. 63, pp. 944-949, 1973.

[23] E. Yamashita, S. Ozeki, and K. Atsuki, "Modal analysis method for optical fibers with symmetrically distributed multiple cores," *J. Lightwave Technol.*, vol. 3, pp. 341-346, Apr. 1985.

[24] K. M. Lo, R. C. McPhedran, I. M. Bassett, and G. W. Milton, "An electromagnetic theory of dielectric waveguides with multiple embedded cylinders," *J. Lightwave Technol.*, vol. 12, pp. 396-410, March 1994.

[25] C. S. Chang and H. C. Chang, "Theory of the circular harmonics expansion method for multiple-optical-fiber system," *J. Lightwave Technol.*, vol. 12, pp. 415-417, March 1994.

[26] T. P. White, B. T. Kuhlmey, R. C. McPhedran, D. Maystre, G. Renversez, C. Martijn De Sterke and L. C. Botten, "Multipole method for microstructured optical fibers. I.Formulation," *J. Opt. Soc. Am. B*, vol. 19, pp. 2322-2330, Oct. 2002.

[27] B. T. Kuhlmey, T. P. White, G. Renversez, D. Maystre, L. C. Botten, C. Martijn de Sterke and R. C. McPhedran, "Multipole method for microstructured optical fibers. II. Implementation and results," *J. Opt. Soc. Am. B*, vol. 19, pp. 2331-2340, Oct. 2002.

[28] S. Campbell, R. C. McPhedran, and C. Martijn de Sterke, "Differential multipole method for microstructured optical fibers," *J. Opt. Soc. Am. B*, vol. 21, pp. 1919-1928, Nov. 2004.

[29] R. Kress, "On the numerical solution of a hypersingular integral equation in scattering theory", *J. Comput. Appl. Math.*, vol. 61, pp. 345-360, Aug. 1995.

[30] D. Colton and R. Kress, *Inverse Acoustic and Electromagnetic Scattering Theory: Second Edition*, Springer-Verlag, 1998.

Wangtao Lu received the B.S. degree in mathematics from the University of Science and Technology of China (USTC), Hefei, China, in 2007. He is currently working toward the Ph.D. degree at the USTC-City University of Hong Kong Joint Advanced Research Center, Suzhou, China.

His current research interests are scientific computation and numerical methods for optical waveguides and photonic crystals.

Ya Yan Lu received the B.S. degree in mathematics from the University of Science and Technology of China, Hefei, China, in 1983 and the Ph.D. degree in applied mathematics from the Massachusetts Institute of Technology, Cambridge, in 1988.

He was a Postdoctoral Researcher with Harvard University, Cambridge, for three years. From 1991 to 1995, he was an Assistant Professor with Rensselaer Polytechnic Institute, Troy, NY. Since 1995, he has been with the Department of Mathematics, City University of Hong Kong, Kowloon, Hong Kong, where he is currently a Professor. His current research interests are numerical analysis, scientific computation, and numerical methods for optical waveguides, photonic crystals and diffraction gratings.